LBNL FORGE Project 3-2535 Report for Milestone 4.3

3D Modeling Studies of Energized Steel-Casing Source Electromagnetic Method for Detecting Stimulated Zone at FORGE Site

Evan Um, David Alumbaugh, Michael Wilt, and Edward Nichols

Earth and Environmental Sciences, Lawrence Berkeley National Laboratory, Berkeley, CA

Introduction

For Project 3-2535, Lawrence Berkeley National Laboratory (LBNL) plans to use an electrically energized casing as an electromagnetic (EM) source at the FORGE site to try and deduce properties of the stimulations including the porosity that is created as well as the size of the reservoir. The proposed EM technique will energize the steel-cased injection (16A) and/or Production (16B) well with an electric current which increases the amount of current within the reservoir. Because the amount of EM signal making it down to the stimulation zone is increased, the method's ability to characterize a deep localized target such as an enhanced geothermal system (EGS) is improved over surface-based EM methods.

This study involves progress that is covered in two earlier milestone reports. First we built a 3D resistivity model (milestone 4.1) derived from the 3D inversion of magnetotelluric data (Wannamaker et al., 2020[a]; Wannamaker et al., 2020[b]). Next we developed a modeling workflow (milestone 4.2) that efficiently and accurately simulates an energized steel-cased well by replacing it with a number of small equivalent current sources. In this report, using the 3D resistivity model and modeling workflow, we simulate several casing source EM configurations and evaluate sensitivity to the stimulated zone. These results will in turn be used to design the EM data acquisition surveys that we will be leading at the FORGE site.

Casing Source EM Configurations

We plan to use three wells for imaging a stimulated zone at the FORGE site, a map of which is provided in Figure 1. The injection well 16A (78)-32 is energized using either top-casing or downhole-casing electric source. As mentioned, the energized casing allows for a higher concentration of electrical currents preferentially flowing along the steel-cased well and directly energizing the stimulated zone at the bottom of the well. The Vertical ElectroMagnetic Profiling (VEMP) system (Miura et al., 1996), a 3-component high-temperature magnetic-field measurement tool that is currently being refurbished for deep borehole deployment at the FORGE site, is simulated as making measurements towards the bottom of observation wells 58-32 and 78B-32. In our current field work plan, we will focus on measuring 3-components magnetic fields. However, in this modeling study we also include calculation of vertical electric fields in the two observation well locations. Though an electric field tool currently does not exist, recent analysis indicates it could be built for as little as $100k. Because electric fields can only be measured in the open well sections of the observation wells, the electric fields are computed at two depths below the casing shoe of well 58-32 which has 100 feet of open hole at the bottom of the well, and a range of positions over 300m at the bottom of well 78B-32. The VEMP tool on the other hand can measure magnetic fields in either open or steel-cased well section. Do to the fact that there currently exists an obstruction that is precluding entrance of the open hole section of well 78B-32 coupled with the fact that we can make measurements in the rest of the cased section, we did not include magnetic field calculations in the open hole section. However, we note that if we are able to get the VEMP tool beneath the cased section of

either of the wells, the magnetic signal will be increased due to a lack of attenuation caused by steel casing.

Figure 2 shows the A-A' and B-B' cross-sectionals of 3D electrical resistivity models prior to (Figure 2a) and after hydraulic stimulation (Figure 2b). Hydraulic stimulation results in an electrically-conductive fluid-saturated zone. For these EM sensitivity studies, we created two different fracture models. In the first case (fracture model 1), we used the DFN modeling results (Finnila, 2021) to determine a percentage of fracture planes in the X, Y and Z directions. This approach yielded more or less isotropic resistivity with values of 302 Ω-m in the X direction (the well axis), 270 Ω-m in the Y direction, and 256 Ω-m in the Z direction. We will refer to this as reservoir model 1. In contrast, in the second case (model 2), we assumed that fluid-filled fractures were oriented only perpendicular to the well axis. This produces an electrically anisotropic reservoir with a resistivity in the X direction of 2970 Ω-m, and in the Y and Z directions the computed resistivity is 190 Ω-m. For more detail on building the reservoir models, the reader is referred to LBNL's FORGE milestone report 4.1.
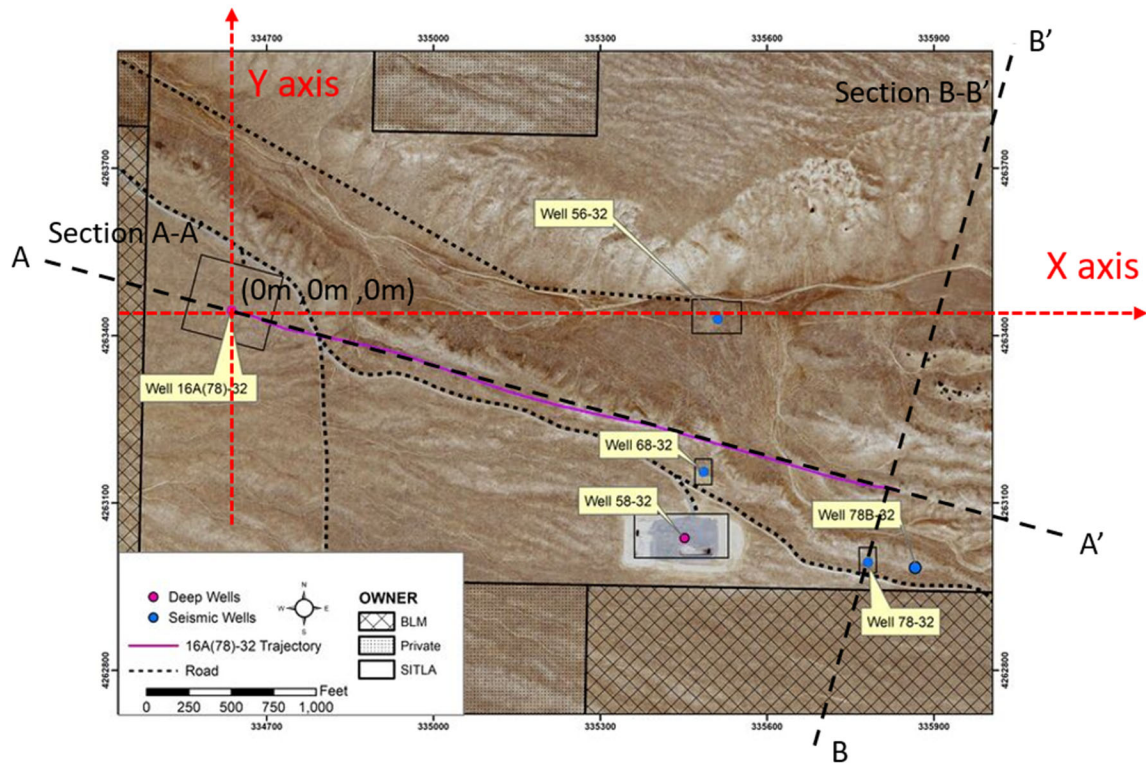
Figure 1. Map view of the Utah FORGE site. The wellhead location of well 16A (78)-32 is set to the center of the coordinates for 3D numerical models.
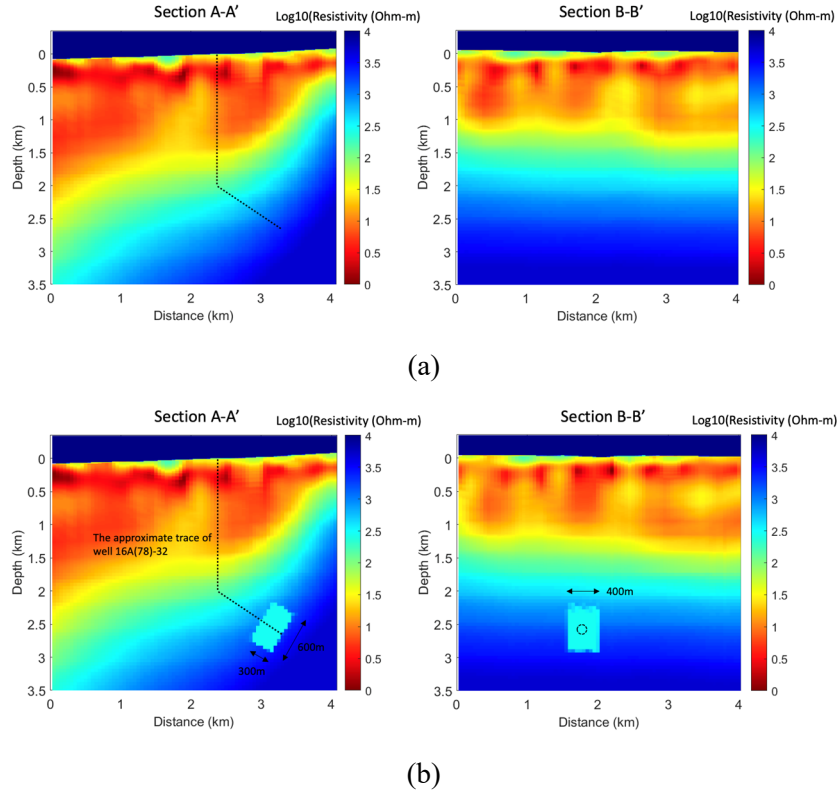
Figure 2. A-A' and B-B' cross-sectionals of the 3D resistivity model (a) prior to and (b) after hydraulic stimulation. The locations of Section A-A' and B-B' relative to the Utah FORGE site are shown in Figure 1. The dotted line in section A-A' represents the approximate trajectory of the 16A (78)-32 well. The top of the well trajectory agrees with the center of the coordinate system shown in Figure 1.

The goal of this work is to examine 1) if the casing source EM configurations can provide at least 10% amplitude anomaly between synthetic data calculated with and without the stimulated zone and 2) if EM field amplitudes are large enough compared to known noise levels to be measurable. For the electric fields we have noise levels of 10^{-8} V/m which is determined by amplifiers used in an E-field measurement system. Recent measurements made with the VEMP tool during the refurbishing process have shown a noise level of 10^{-14} T for the component of magnetic fields made in the direction of the tool's axis (i.e., the vertical field is a vertical well), and 10^{-13} T for the horizontal magnetic fields. The axial field has lower noise levels as the sensor consists of a single-long high sensitivity induction coil, while the horizontal components have poorer noise levels due to the fact that the sensors consist of a series of short (~3") induction coils stacked in series.

Figure 3 shows the three casing source EM configurations examined in this report. The top-casing source configuration (Figure 3a, Marsala et al., 2014) uses a surface electrode. One end of the electric source energizes a wellhead and the other is placed on the surface sufficiently away from the well. The injected current flows down along the steel-cased injection well to depth. In the down-hole source configuration (Figure 3b, Marsala et al., 2014), one electrode is directly connected to the casing within the well at depth while the other electrode is placed on the surface sufficiently away from the well. Compared to the top-casing source configuration, the down-hole source configuration can illuminate a deeper target at the expense of a well intervention procedure. The third source configuration (Figure 3c, Cuevas 2014) uses a finite-long (20m) vertical electric dipole source inside the cased well.

3
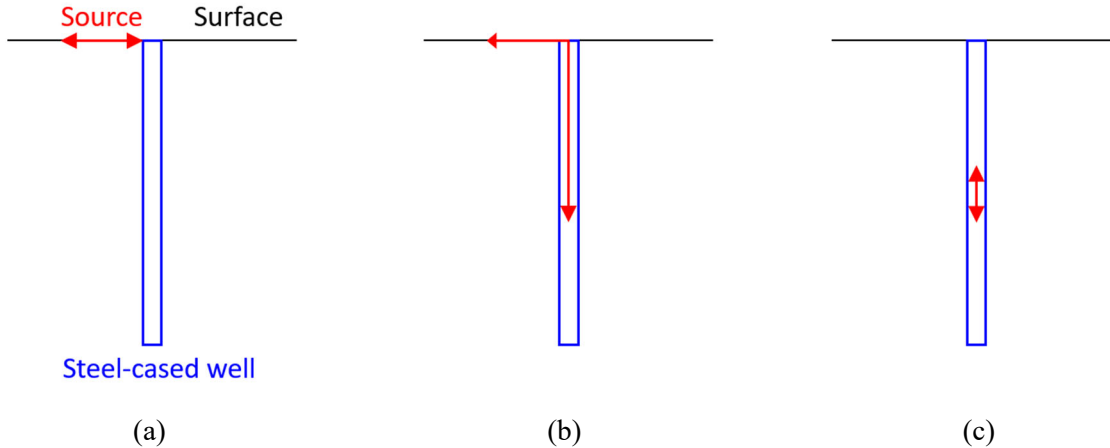
Figure 3. Casing source EM configurations. (a) The top-casing source configuration. (b) The down-hole source configuration. (c) The vertical electric dipole source inside the cased well.

Numerical Modeling Results

Using the casing modeling workflow (LBNL's FORGE milestone 4.2 report) and 3D finite element modeling codes (Um et al., 2020), we simulated the casing-source EM responses to the FORGE resistivity models (LBNL's FORGE milestone 4.1) before and after hydraulic stimulation. Figure 4 shows the layout of the surface source that we employed in this study for source configurations given by Figure 3a and 3b relative to the 16A well head, the surface projection of the deviated section of well 16A, and the relative location of the two observation wells where the VEMP and hypothetical electric field borehole tools would be deployed. For the results presented below, frequencies of 5Hz and 50Hz were employed, the source current amplitude was set to one Ampere, and the EM receiver moment was also set to unity. In terms of measurement levels that would be made in the field, they will be larger in magnitude compared to the values reported here as experience has shown that we will likely be able to transmit at least 5 to 20 Amperes into the casing source.

In terms of numerical simulation of the VEMP receiver, we have taken into account the attenuating effects of steel casing on magnetic field measurements by multiplying the magnetic field solutions by a casing attenuation coefficient read from the figures in Wu and Habashy (1994) shown in Figure 5. Note that we have assumed that most of the VEMP measurements will be made in steel casing and a correction was applied during the data processing stage at the time of this study. It is assumed it will be difficult to get into the open hole section of well 78B-32 due to a protrusion of some sort at the casing shoe. If that protrusion is drilled out prior to deployment of our logging system, this will open up a greater range of VEMP measurements with respect to depth, as well as for the possible deployment of an electric field measurement should we be able to secure the funding to build an electric field receiver.

1) The top-casing source configuration

Figure 6 below shows the computed X, Y, and Z components of the magnetic fields for a source frequency of 5Hz, while Figure 7 shows the results at 50Hz. Despite the attenuating effect of the casing Figures 6 and 7 indicate that the predicted magnetic field amplitudes are several orders of magnitude larger than the measure noise floors (i.e., 10^{-14} T for vertical magnetic fields and 10^{-13} T for horizontal magnetic fields). Note that at 5 Hz (Figure 6) here is little sensitivity to the stimulated zone, while at 50Hz (Figure 7) there is a significant reservoir response. It is also worth to mention that various

components magnetic field measurements can distinguish the isotropic fracture zone (fracture model 1) from the anisotropic scenario (fracture model 2).
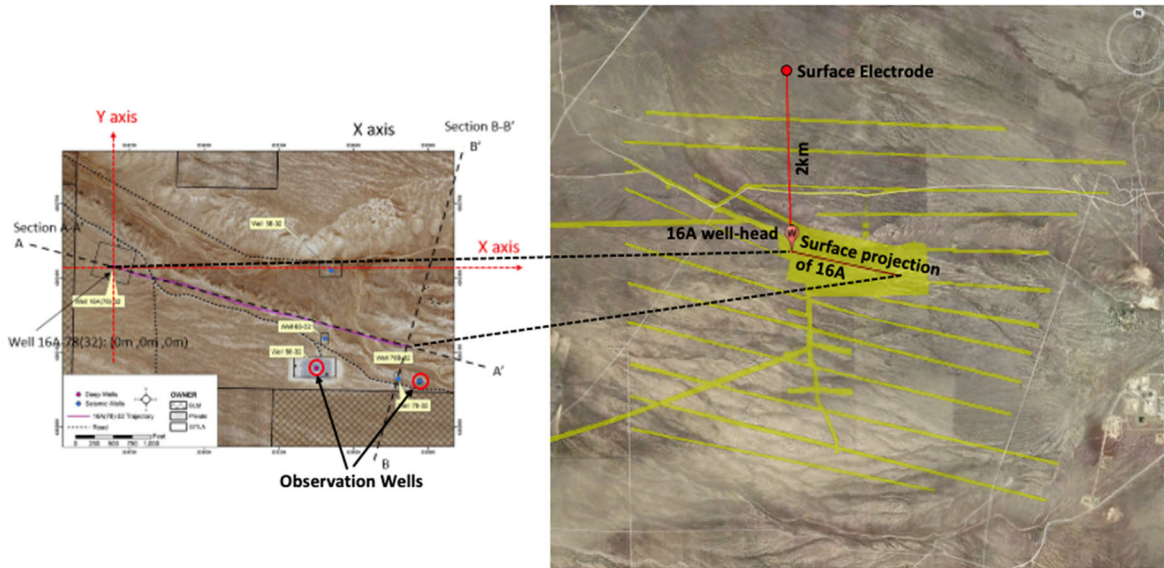
Figure 4. Map showing the details of the source and receiver positions used in the EM numerical modeling survey design study. The tight figure shows the surface layout of the source with the return electrode to the north, as well as the wellhead and surface projection of the deviated part of well 16A. The map view on the left is the same as in Figure 1 and shows the location of the observation wells in the simulation as red circles (58-32 on the left and 78B-32 on the right) relative to the surface projection of the deviated portion well 16A.
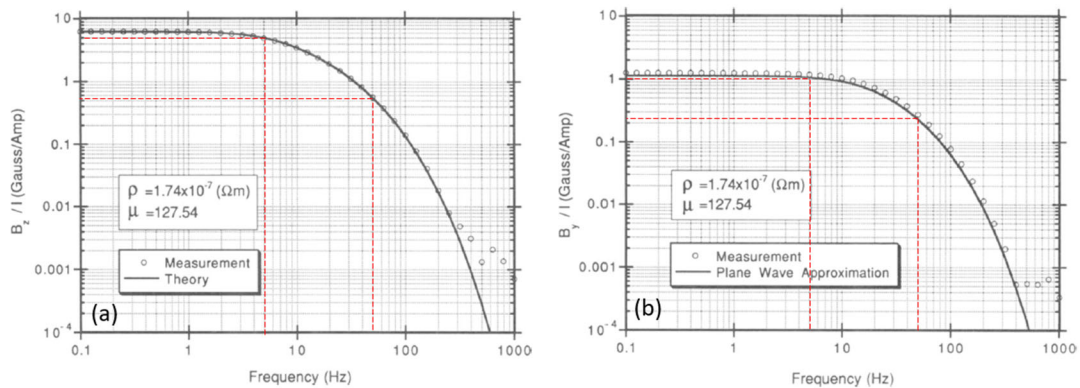
Figure 5. The attenuation effect of steel well casing (geometry: 9.5mm thick, 14cm outer diameter) on magnetic field measurements inside the well (Wu and Habashy, 1994). (a) The transverse electric mode. (b) the transverse magnetic mode. The red broken lines indicate the casing attenuation at 5 and 50 Hz.
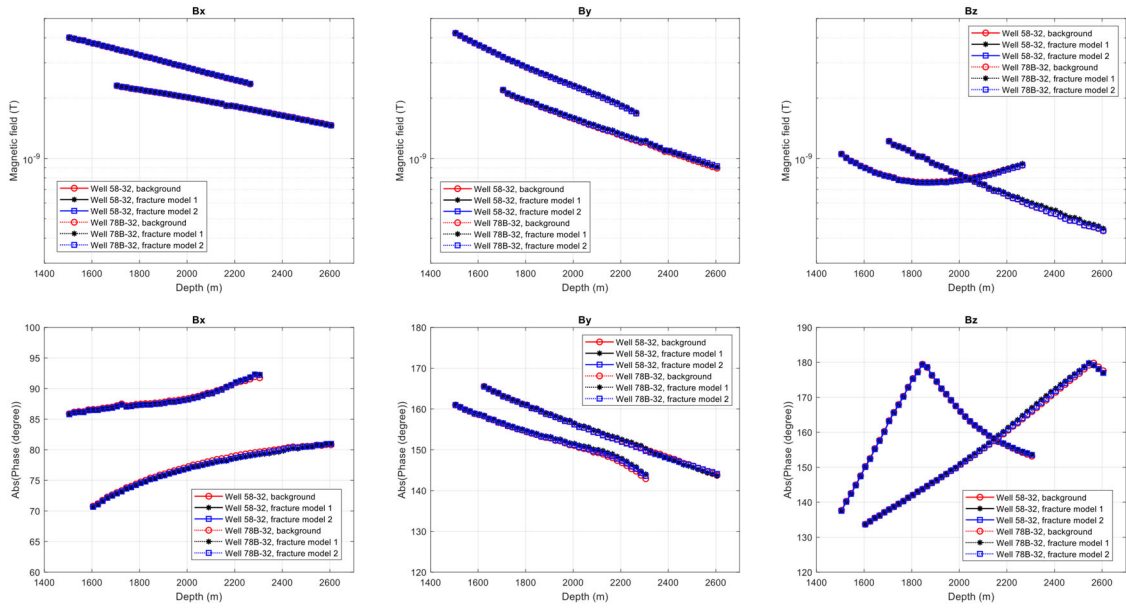
Figure 6. Borehole VEMP measurements using the top-casing source configuration and a source frequency of 5Hz. The three columns correspond to the X, Y, and Z components of the magnetic field, respectively. The top row displays the amplitude of each component, and the bottom row the phase.
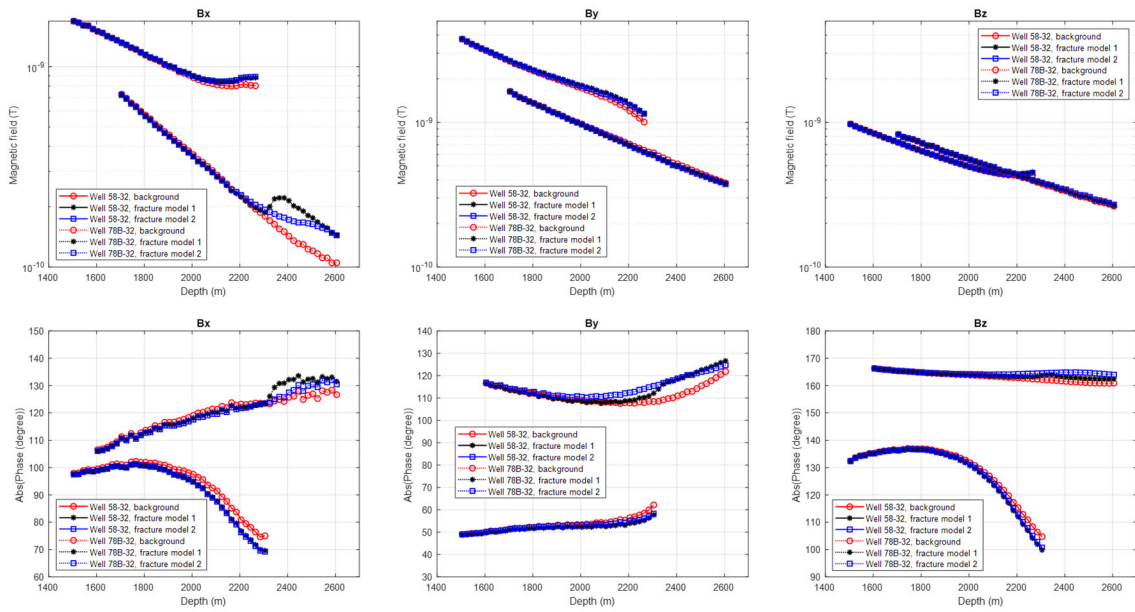
Figure 7. Borehole VEMP measurements using the top-casing source configuration and a source frequency of 50Hz. The three columns correspond to the X, Y, and Z components of the magnetic field, respectively. The top row displays the amplitude of each component, and the bottom row the phase.

Figure 8 shows the percent differences between the two fracture models and the background model. Note that as expected, the 5Hz results in Figure 8a do not show anomalies generated by the stimulation that exceed 10% which is the minimum sensitivity threshold to proceed with field measurements. However, at 50Hz, the Bx component does exceed this threshold though the lower-noise vertical component does not. Because of this, the remainder of this report will focus on the 50Hz results except where noted. Also, the sensitivity to parallel-fracture anisotropic reservoir versus an isotropic case is clearly demonstrated in these results.

(a)

(b)
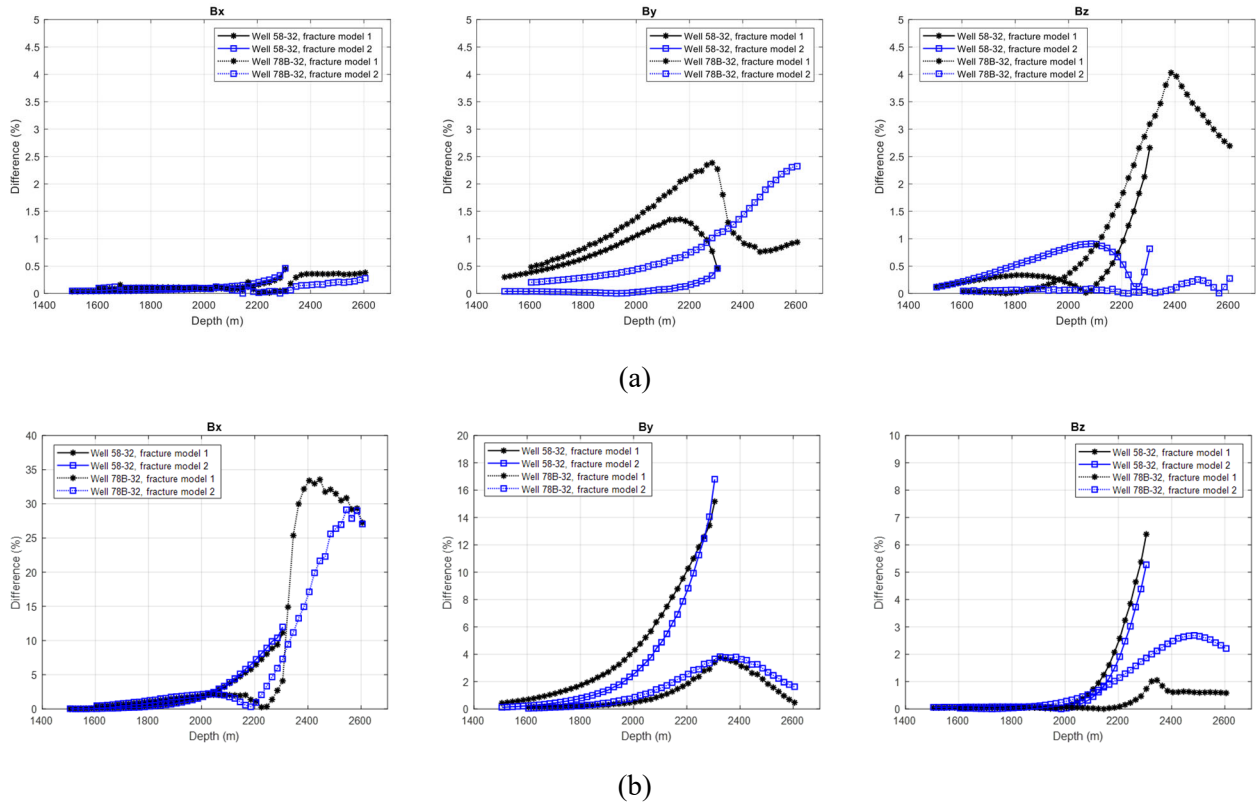
Figure 8. The percent differences in the borehole magnetic field amplitudes between the baseline and fractured reservoir modeling results. The wellhead is excited using the top-casing source, and the three columns correspond to the X, Y, and Z components of the magnetic field, respectively. (a) Differences for the 5Hz results shown in Figure 6. (b) Differences for the 50Hz results shown in Figure 7.

Figure 9 shows vertical electric fields that would be measured at the two frequencies in the open well sections of the two observation wells. Note that because well 58-32 has only 100 feet of open hole section, it is assumed that only two electric field measurement points could be made in this well. Compared to the magnetic field measurements (Figures 6 through 8), the borehole electric field measurements are highly sensitive to the stimulated zone at both frequencies, and the results clearly distinguish between the three models. The amplitude at both frequencies generally is higher than a typical noise floor of and electric field measurement which we assume to be 10^{-8} V/m, though some of the 50Hz results are close to this noise-floor level. As mentioned earlier, in this modeling study the source current is set to one Ampere, while in practice, we would likely be able to put in 5~20 Amperes. In addition, if

we were to build an electric field measurement system, the receiver length would be 5 to 10m long which would further increase the amplitude of the measured signal. Thus, if an electric field measurement system were to be built and deployed at the Utah FORGE site, we expect that borehole electric field amplitudes will be sufficiently large to provide for high quality measurements.
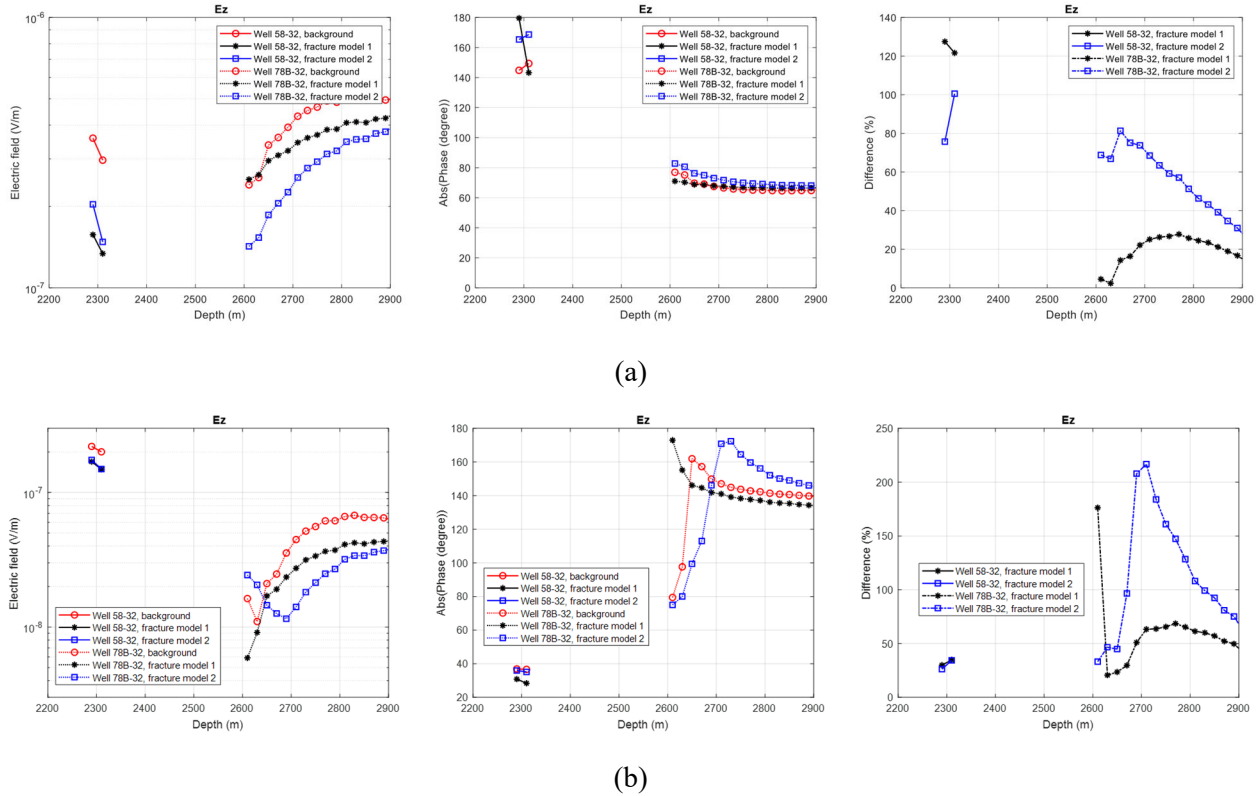
Figure 9. Calculated vertical electric field amplitudes (left) and phases (center) in the open-hole sections of the two observations wells. The right-hand figures show the percent differences between the background and two fracture models. The wellhead is excited using the top-casing source. (a) 5Hz results. (b) 50Hz results.

2) The down-hole source configuration

For the down-hole source configuration, one source electrode is connected to the injection well at depth and the return electrode is grounded 2km away from the wellhead as shown in Figure 4. We consider three different downhole source positions within the vertical section of well 16A: 0.5km, 1km and 1.5 km depth. As mentioned above, due to a lack of sensitivity at 5Hz we will focus the rest of this report on the results calculated at 50 Hz. Except for the down hole source position, all other modeling parameters are the same as those used for the top-casing source configuration. Figures 10 and11, show the three-component magnetic fields and corresponding percent differences between the two fracture and background models when the source is placed at z=0.5 km depth in well 16A. Figure 12 shows the corresponding vertical electric field measurements in the open-hole sections of the two observation wells. Both magnetic and electric field amplitudes are sufficiently larger than the previously mentioned sensor

noise levels. The horizontal magnetic fields show the amplitude anomalies exceeding the minimum sensitivity (10%), and as before the vertical electric field measurements greater sensitivity to the fractured reservoir compared to the magnetic fields. Also note that the magnitude of the percent-difference anomalies is larger for the downhole source than for the surface connection assumed in Figures 8 and 9. Last, note that both magnetic and electric field measurements continue to distinguish the isotropic reservoir model from the anisotropic one.
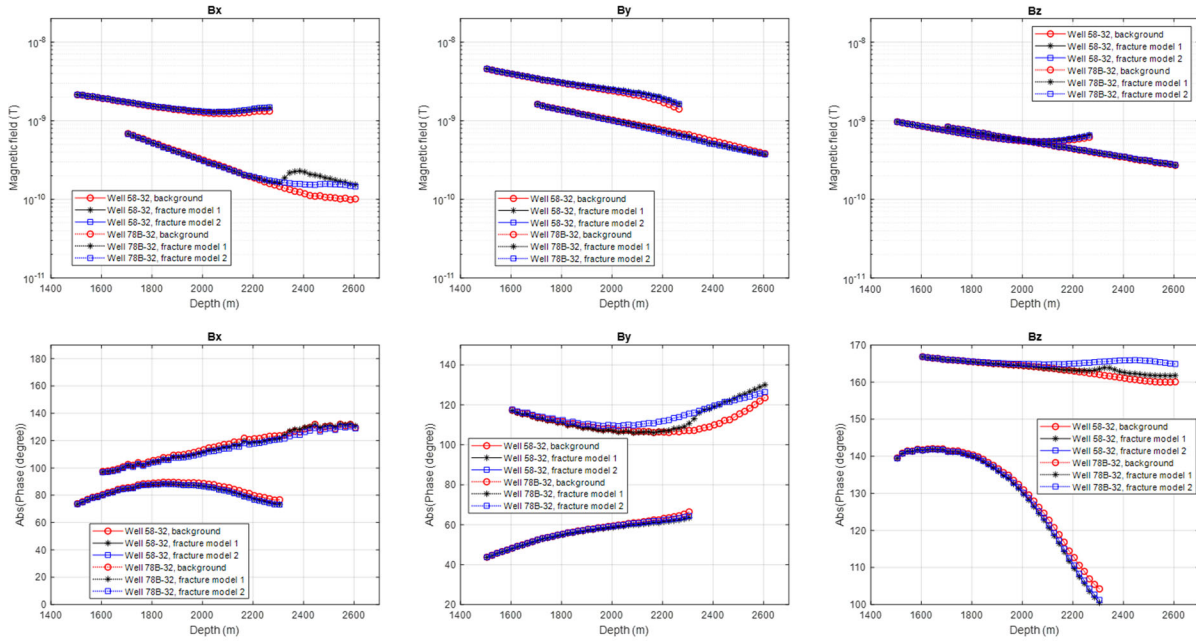
Figure 10. Borehole VEMP measurements using downhole connection depth of 500m in well 16A and a source frequency of 50Hz. The three columns correspond to the X, Y, and Z components of the magnetic field, respectively. The top row displays the amplitude of each component, and the bottom row the phase.
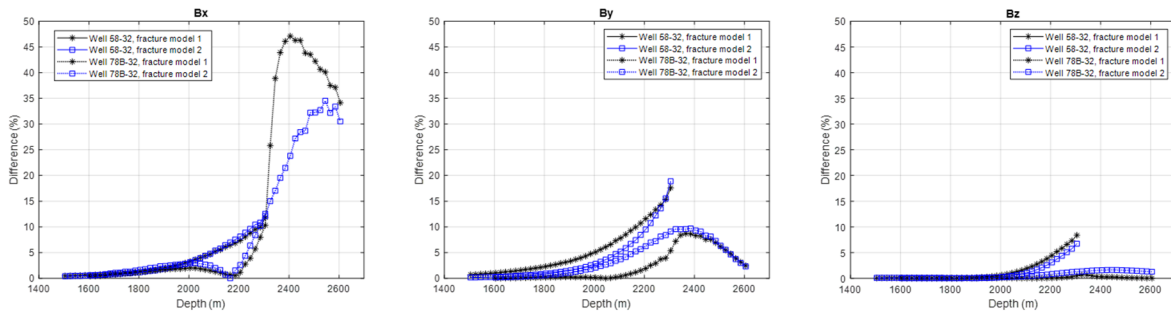
Figure11. The percent differences in the borehole magnetic field amplitudes between the baseline and fractured reservoir modeling results for the 50Hz results shown in Figure 10. The well is excited using a connection at 500m depth, and the three columns correspond to the X, Y, and Z components of the magnetic field, respectively.

9
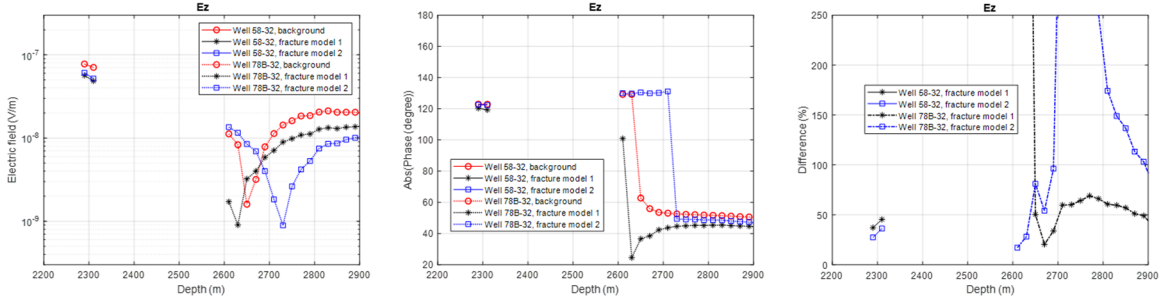
Figure 12. Calculated vertical electric field amplitudes (left) and phases (center) in the open-hole sections of the two observations wells. The right-hand figures show the percent differences between the background and two fracture models. The well is excited using a connection at 500m depth, and the frequency is 50Hz.

We repeat simulating borehole EM measurements using in-well source connection depths of 1 km and 1.5 km. Figures 13-15 show the EM measurements and percent differences in amplitude between the stimulated-reservoir and background models when the source is placed at z=1 km. Both the overall signal strength as well as the sensitivity to the zone of stimulation are enhanced compared to both of the previous source configurations, that is, the results for the connection to the well at the surface and at z=0.5 km. The horizontal magnetic field measurements provide up to 80% amplitude anomaly between the background and fracture models, sufficiently exceeding the sensitivity required for borehole EM imaging. In contrast, the vertical magnetic fields are still less sensitive to the stimulated zone. The vertical electric field measurements (Figure 15) are also well above estimated sensor noise levels and highly sensitive to the stimulated zone.
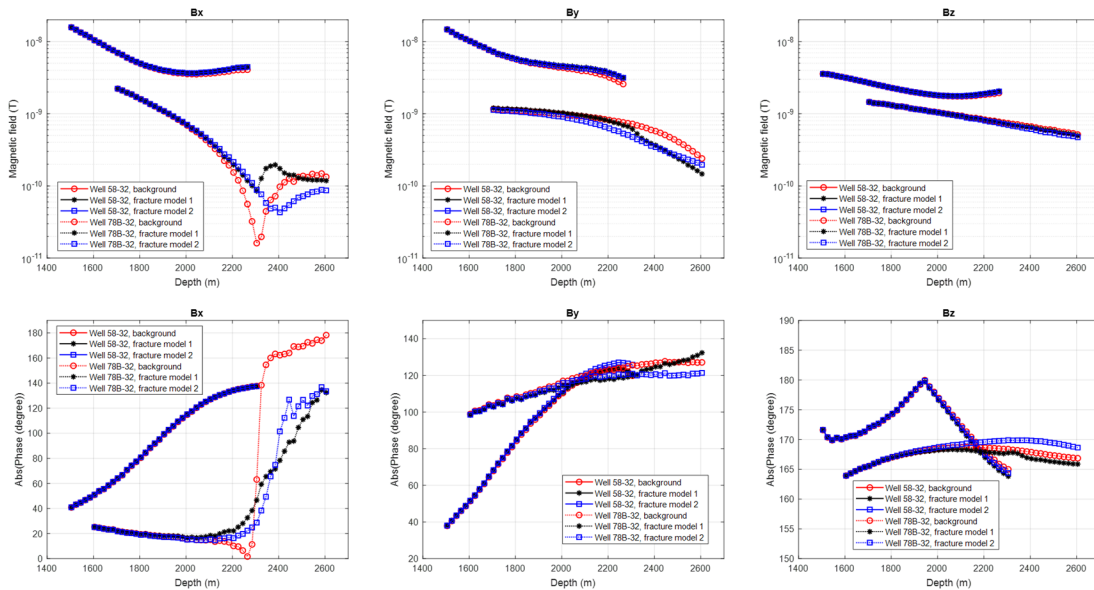
Figure 13. Borehole VEMP measurements using downhole connection depth of 1km in well 16A and a source frequency of 50Hz. The three columns correspond to the X, Y, and Z components of the magnetic field, respectively. The top row displays the amplitude of each component, and the bottom row the phase.
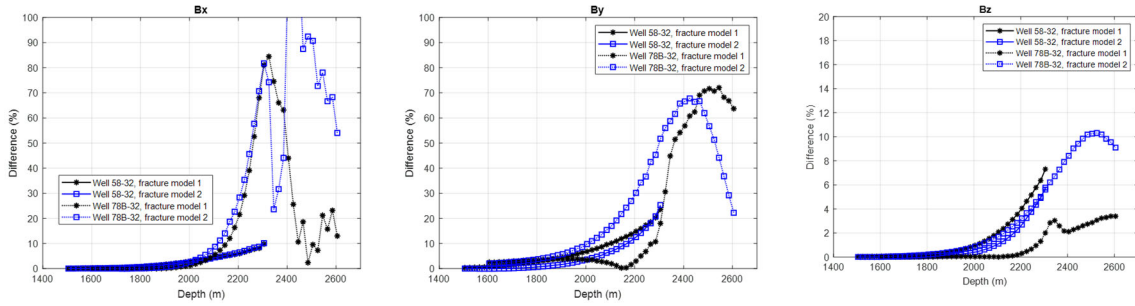
Figure14. The percent differences in the borehole magnetic field amplitudes between the baseline and fractured reservoir modeling results for the 50Hz results shown in Figure 13. The well is excited using a connection at 1 km depth, and the three columns correspond to the X, Y, and Z components of the magnetic field, respectively.
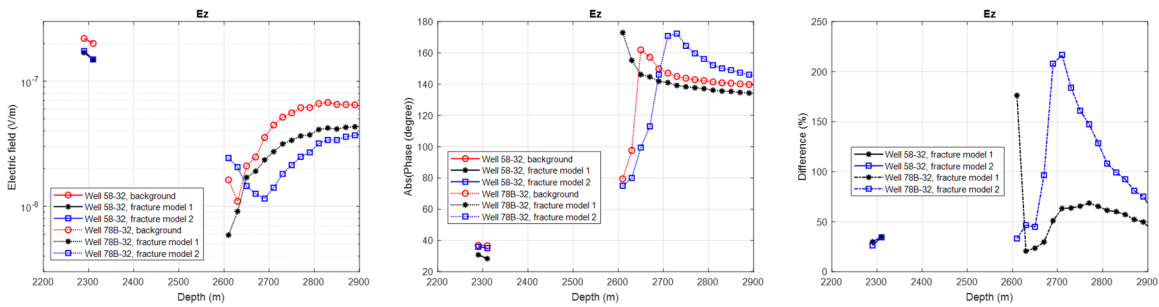
Figure 15. Calculated vertical electric field amplitudes (left) and phases (center) in the open-hole sections of the two observations wells. The right-hand figures show the percent differences between the background and two fracture models. The well is excited using a connection at 1 km depth, and the frequency is 50Hz.

Next, the downhole source is placed at a depth of 1.5 km, the deepest position used in this study. Unlike the previous two down-hole source configurations where the source is placed in the electrically conductive basin sediments, the source now is placed in highly resistive granite basement. The resulting magnetic and electric field measurements and respective anomalies are plotted in Figures 16-18. The EM measurements show detectable anomalies but the anomaly amplitudes in the horizontal components are decreased compared to the previous examples simulated using the source at z=1 km. At the same time the anomaly in the vertical component has increased from 10% previously to 30% in this case for the anisotropic model. Perhaps, a higher source frequency would be required for improving the sensitivity to the fracture zones when the source is placed in such a resistive environment. However, we refrain ourselves from doing additional modeling analysis at higher frequencies due to 1) difficulties associated with modeling steel-casing effects at higher frequencies and 2) 600-700m limit of the high-temperature logging cables currently available to the LBNL team for deployment in wells 16A and 16B.

11
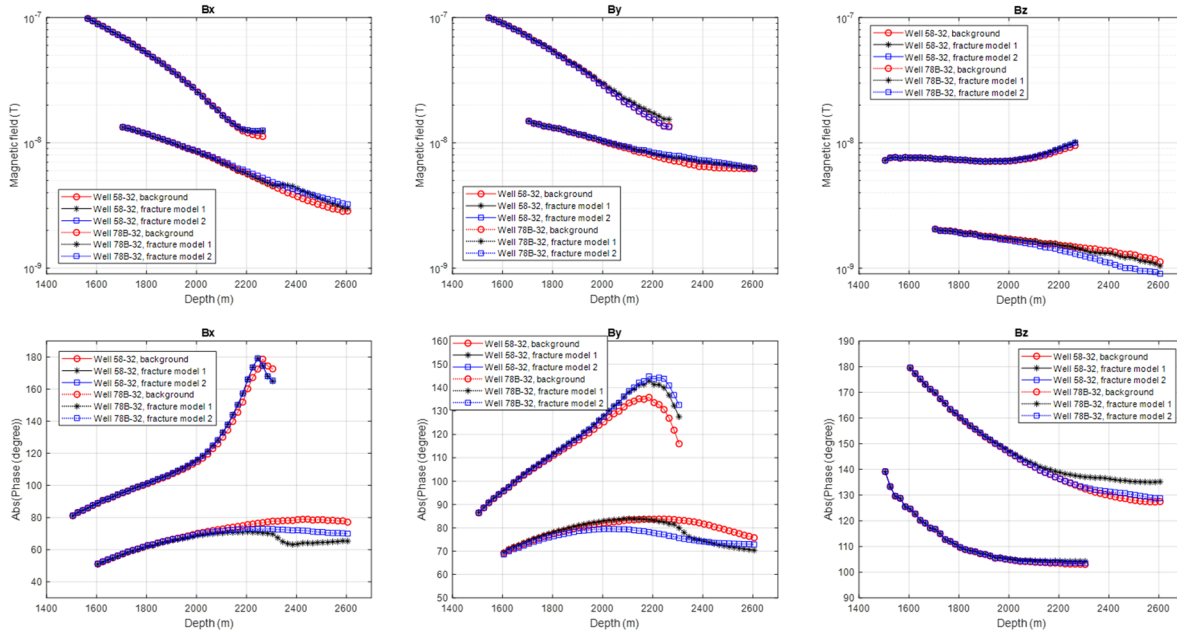
Figure 16. Borehole VEMP measurements using downhole connection depth of 1.5 km in well 16A and a source frequency of 50Hz. The three columns correspond to the X, Y, and Z components of the magnetic field, respectively. The top row displays the amplitude of each component, and the bottom row the phase.
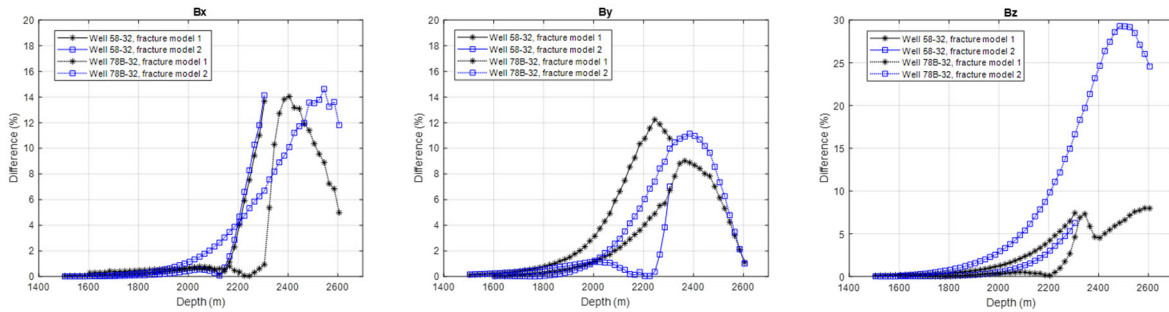
Figure17. The percent differences in the borehole magnetic field amplitudes between the baseline and fractured reservoir modeling results for the 50Hz results shown in Figure 16. The well is excited using a connection at 1.5 km depth, and the three columns correspond to the X, Y, and Z components of the magnetic field, respectively.
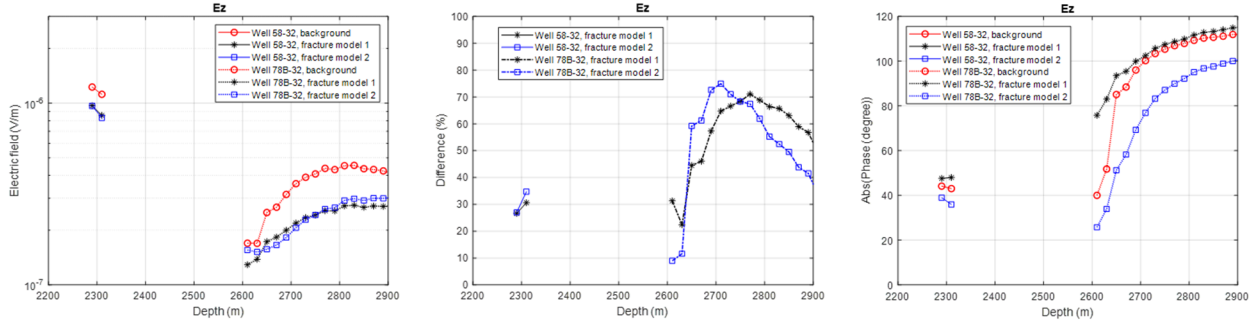
Figure 18. Calculated vertical electric field amplitudes (left) and phases (center) in the open-hole sections of the two observations wells. The right-hand figures show the percent differences between the background and two fracture models. The well is excited using a connection at 1.5 km depth, and the frequency is 50Hz.

3) The vertical electric dipole source configuration

In this configuration, a 20m long vertical electric dipole (VED) source is placed at z=1.5 km inside and energizes the steel-cased injection well. The source frequency is again set to 50 Hz. The resulting magnetic (Figures 19 and 20) and electric (Figure 21) fields exhibit amplitudes that are relatively small compared to those from the other casing source configurations because of the smaller source moment that 20m long VED source has compared to a long surface-to-borehole source such as those configurations outlined above. Nonetheless, the proposed VED source still yields measurable EM field amplitudes above the noise floor, and the percent differences in the vertical EM fields between the background and fracture models exceed the sensitivity requirement (i.e., 10% amplitude anomaly) for borehole EM imaging.

Summary and Future Work

Our 3D numerical modeling results indicate that 1) the borehole VEMP measurements are sensitive to the anticipated stimulated zone in terms of producing at least a 10% anomaly between models with and without the stimulated reservoir and 2) the EM amplitudes sufficiently exceed the measured noise levels of the various sensors. We have evaluated three different casing source configurations coupled with the VEMP system. Among them, our choice for an optimal source configuration would be the downhole located at or between 500m to 1.0km depth as it provides the largest amplitude anomaly over a range of VEMP positions. At this point, we have not built a borehole sensor for measuring vertical electric fields due to current lack of funding. However, our numerical modeling studies suggest that the vertical electric field measurements are highly sensitive to the stimulated zone and can be used as additional constraints for detecting and imaging the reservoir. The LBNL team is currently formulating a budget for developing the electric field sensor in a high-temperature borehole environment, and have estimated it will cost around $135k to do so.

We believe the modeling and sensitivity study presented here warrant a 'GO' decision moving forward. Additional modeling will be undertaken to 1) understand how magnetic permeability of the steel casing used to complete the injection and production wells affects the measured field strength and resulting anomalies, and 2) determine if changing the location of the surface electrode provides additional information. Pending approval from the Utah FORGE management and technical advisory team, our

plans are to deploy the system and make a suite of measurements at the site in the Fall of 2023 just prior to the planned simulation, and just after the stimulation has been completed.
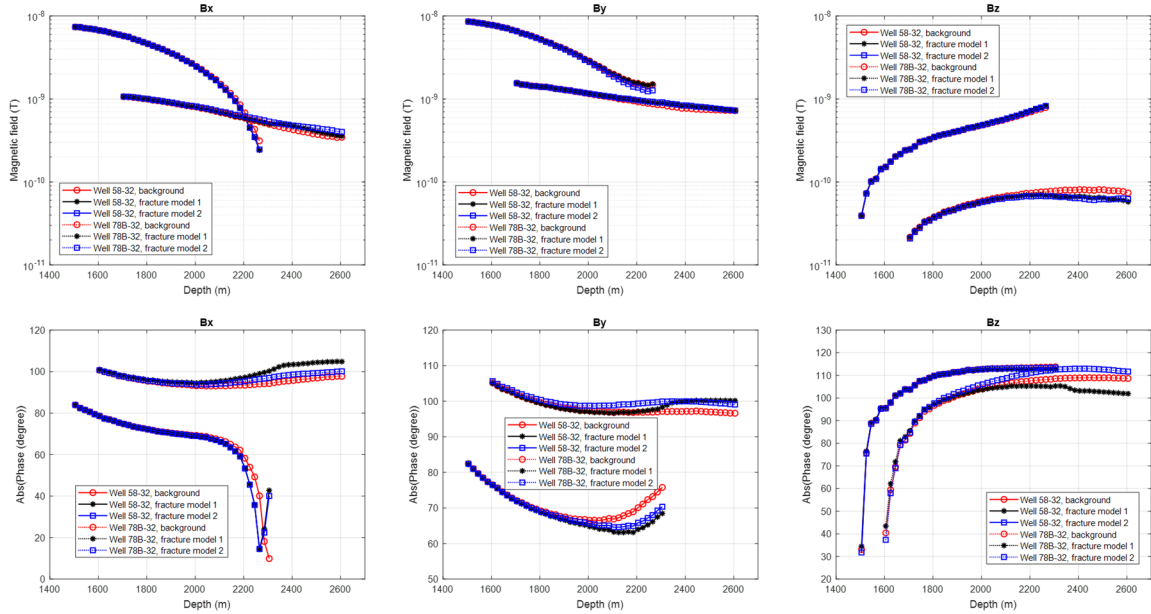
Figure 19. Borehole VEMP measurements using 20m long electric dipole source at 1.5 km depth in well 16A and a source frequency of 50Hz. The three columns correspond to the X, Y, and Z components of the magnetic field, respectively. The top row displays the amplitude of each component, and the bottom row the phase.
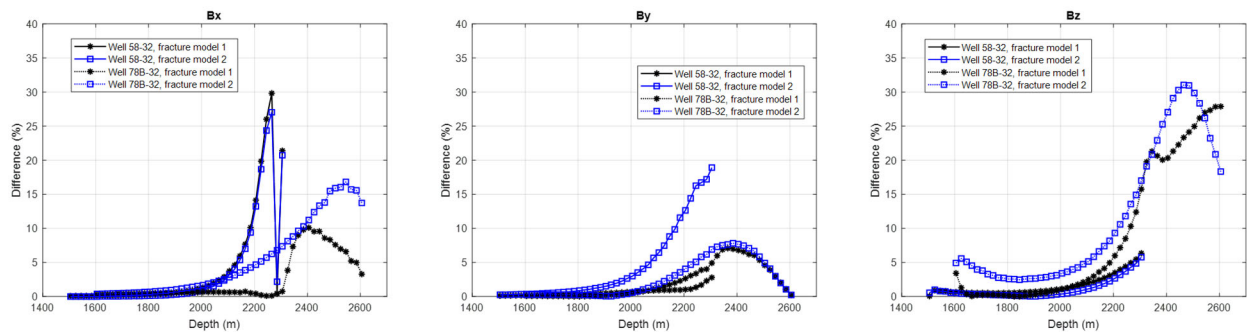
Figure 20. The percent differences in the borehole magnetic field amplitudes between the baseline and fractured reservoir modeling results for the 50Hz results shown in Figure 19. The well is excited using a 20m long electric dipole source centered at 1.5 km depth, and the three columns correspond to the anomalies X, Y, and Z components of the magnetic field, respectively.

14
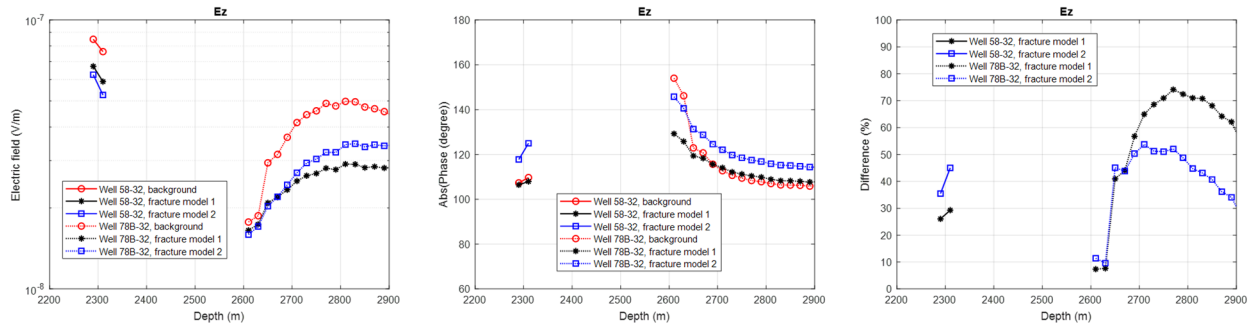
Figure 21. Calculated vertical electric field amplitudes (left) and phases (center) in the open-hole sections of the two observations wells. The right-hand figures show the percent differences between the background and two fracture models. The well is excited using a 20m long electric dipole source centered at 1.5 km depth, and the frequency is 50Hz.

References

Cuevas, N.H., 2014. Analytical solutions of EM fields due to a dipolar source inside an infinite casing. Geophysics, 79(5), pp. E231-E241.

Finnila, Aleta, FORGE DFN model file availability on the GDR, FORGE Modeling and Simulation Forum, July 21, 2021, https://utahforge.com/wp-content/uploads/sites/96/2021/07/MandS_Forum8-AFinnila-July2021.pdf

Marsala AF, Hibbs AD, Morrison HF. Borehole casing sources for electromagnetic imaging of deep formations. InSPE Annual Technical Conference and Exhibition 2014 Oct 27. OnePetro.

Miura, Y., Osato, K., Takasugi, S., Muraoka, H. and Yasukawa, K., 1996. Development of the Vertical Electro Magnetic Profiling (VEMP) method. Journal of applied geophysics, 35(2-3), pp.191-197.

Um, E.S., Kim, J. and Wilt, M., 2020. 3D borehole-to-surface and surface electromagnetic modeling and inversion in the presence of steel infrastructure. Geophysics, 85(5), pp.E139-E152.

Wannamaker, P.E., Simmons, S.F., Miller, J.J., Hardwick, C.L., Erickson, B.A., Bowman, S.D., Kirby, S., Feigl, K.L. and Moore, J.N., 2020[a]. Geophysical Activities over the Utah FORGE Site at the Outset of Project Phase 3. Stanford, California, Stanford University, Proceedings, 45th Workshop on Geothermal Reservoir Engineering.

Wannamaker, Phil, Maris, Virginia. *Utah FORGE: Phase 3 Magnetotelluric (MT) Data*. United States: N.p., 01 Oct, 2020[b]. Web. doi: 10.15121/1776598.

Wu, X. and Habashy, T.M., 1994. Influence of steel casings on electromagnetic signals. Geophysics, 59(3), pp.378-390.